Genome-wide screening reveals producer-cell modifications that improve virus-like particle production and delivery potency

Diana Ly[1], Hyewon Jang[1], Adhiraj Goel[1], Arnav Singh[1], Aditya Raguram[1,2]*

[1] Whitehead Institute for Biomedical Research, Cambridge, MA, USA

[2] Merkin Institute for Transformative Technologies in Healthcare, Broad Institute of MIT and Harvard, Cambridge, MA, USA

* Correspondence: araguram@wi.mit.edu (A.R.)

Abstract

Engineered virus-like particles (eVLPs) are promising vehicles for transient delivery of gene editing agents. While extensive particle optimization has yielded efficient eVLPs, it remains underexplored whether engineering the cells used to produce eVLPs could further improve eVLP properties. We developed a genome-wide screening approach to systematically investigate how genetic perturbations in producer cells influence eVLP production, and we applied this approach to identify several genes that regulate eVLP cargo expression and loading into particles during the production process. Leveraging these insights, we engineered producer cells that support increased eVLP cargo packaging and a 2- to 9-fold increase in eVLP delivery potency across several cargo, particle, and target-cell types in cultured cells and in mice. Our findings suggest the potential of producer-cell engineering as a useful strategy for improving the utility of eVLPs and related delivery methods.

Methods for safely and efficiently delivering macromolecules into cells in culture (*in vitro*) and within the body (*in vivo*) are required for many therapeutic strategies, including gene editing therapies[1-5]. Recently, virus-like particles (VLPs) have emerged as promising vehicles for therapeutic macromolecule delivery that combine key advantages of canonical viral and non-viral delivery strategies[1,6]. In typical VLPs, viral scaffold proteins are used to package and deliver cargo proteins, ribonucleoproteins (RNPs), or mRNAs instead of viral genetic material, which leads to transient cargo delivery into recipient cells[1,6]. Several VLP-based delivery methods have proven particularly effective for gene editing applications[7-23] and offer an ideal combination of efficient on-target editing, minimal off-target editing, and programmable cell-type targeting capabilities. Current state-of-the-art VLPs, including engineered VLPs (eVLPs)[7,8,22], have achieved efficient *in vitro* gene editing in primary human cells and therapeutic *in vivo* gene editing in the mouse liver and retina, highlighting the utility of eVLP delivery for research and potential therapeutic applications.

While extensive engineering of eVLP components and particle architectures has afforded efficient eVLPs[7,8,22], further improvements to eVLP properties are still required to maximize their prospects for clinical translation. In particular, improving eVLP cargo packaging per particle or overall particle yield from the eVLP production process would enable more efficient gene editing with lower eVLP doses and simplify the production of eVLPs for large-scale studies. Standard methods for producing eVLPs involve the use of human producer cells to express eVLP components and assemble functional particles[7,8,22], suggesting that producer cells likely play an important role in the eVLP production process. However, previous studies have focused solely on particle engineering to improve eVLP properties, and none have explored whether producer-cell engineering could improve eVLP properties beyond what can be achieved through particle engineering alone. In this study, we systematically investigated how genetic perturbations in producer cells influence eVLP production and applied our findings to engineer producer cells that support improved eVLP production and delivery potency.

We began by developing an unbiased genome-wide screening approach to identify genetic perturbations in producer cells that influence eVLP production (Fig. 1a). We envisioned a general scheme in which eVLP production is initiated from a pool of

genetically perturbed producer cells. Each producer cell in this pool expresses a Cas9-based genome modifying agent and a single copy of a guide RNA (sgRNA) that directs the installation of a specific genetic perturbation into that particular cell (Fig. 1a). Because eVLPs package Cas9-based cargos, the perturbation-inducing sgRNA expressed in a given producer cell is also loaded into any particles produced by that particular cell (Fig. 1a). Therefore, the abundance of a particular sgRNA in eVLPs reflects how the corresponding genetic perturbation influences eVLP production or cargo loading: sgRNAs that are more abundant identify perturbations that increase eVLP production or cargo loading, while sgRNAs that are less abundant identify perturbations that decrease eVLP production or cargo loading (Fig. 1a).

We used this general approach to perform a genome-wide knockout screen for cargo-loaded eVLP production in Gesicle 293T producer cells, a standard cell line used for eVLP production[7,8,22]. We transduced producer cells at a low multiplicity of infection (MOI) with a lentiviral sgRNA library containing 98,077 unique sgRNAs targeting 19,707 genes across the human genome[24] (Extended Data Fig. 1a). Each vector in the library also encoded constitutive expression of Cas9 nuclease. After selecting for Cas9 expression and expanding the transduced cells to generate a pool of single-knockout producer cells, we initiated fourth-generation (v4) base editor (BE)-eVLP production from these cells (Extended Data Fig. 1a). Importantly, to initiate eVLP production, we only transfected plasmids encoding the expression of adenine base editor (ABE8e)-packaging v4-eVLP protein components: (1) the gag–ABE (capsid–cargo) fusion, (2) the Moloney murine leukemia virus (MMLV) gag–pro–pol polyprotein, and (3) the vesicular stomatitis virus G (VSV-G) envelope protein. No additional sgRNA-encoding plasmid was transfected, ensuring that all eVLPs produced from a given producer cell packaged cargo containing the specific knockout-inducing sgRNA that was already introduced into that producer cell by lentiviral transduction (Fig. 1a and Extended Data Fig. 1a).

Following eVLP production, we isolated RNA from purified eVLPs and compared this eVLP-packaged RNA to cellular RNA that was isolated from the single-knockout producer-cell pool immediately prior to eVLP production (Fig. 1a and Extended Data Fig. 1a). To compare sgRNA abundances across both populations, we subjected both RNA pools to template-switching reverse transcription[25], which enabled amplification and

86 sequencing of the spacer sequence at the 5' end of each sgRNA molecule (Extended
87 Data Fig. 1b). sgRNAs that are more abundant in the eVLP-packaged RNA compared to
88 the producer-cell RNA identify gene knockouts that increase eVLP production or cargo
89 loading, while sgRNAs that are less abundant identify gene knockouts that decrease
90 eVLP production or cargo loading (Fig. 1a and Extended Data Fig. 1a).

91 By aggregating the results for all sgRNAs targeting the same gene into gene-level
92 phenotypes, we determined the effect of each producer-cell gene knockout on eVLP
93 production or cargo loading (Fig. 1b and Extended Data Fig. 1c). We observed that the
94 majority of gene knockouts did not substantially impact eVLP production or cargo loading,
95 some knockouts decreased eVLP production or cargo loading, and very few knockouts
96 increased eVLP production or cargo loading (Fig. 1b). These results are consistent with
97 a model in which there are more genes in producer cells that positively regulate eVLP
98 production than genes that negatively regulate eVLP production. Taken together, the
99 results of this genome-wide knockout screen illuminate the producer-cell determinants of
100 eVLP production and nominate several gene knockouts ("hits") that appear to strongly
101 impact eVLP production or cargo loading (Fig. 1b).

102 Next, we sought to characterize the gene knockouts that most strongly decreased
103 eVLP production or cargo loading. The three strongest negative hits from our screen—
104 *MPP8*, *TASOR*, and *MORC2*—are all associated with the human silencing hub (HUSH)
105 complex, which is responsible for epigenetically silencing intronless transgenes, including
106 retroviral elements[26,27]. We first individually validated each negative hit by measuring the
107 relative sgRNA abundance in eVLPs produced from *MPP8*-, *TASOR*-, or *MORC2*-
108 knockout cells (hereafter collectively referred to as HUSH-knockout cells) compared to
109 eVLPs produced from standard producer cells. To independently generate each knockout
110 cell line, we mimicked the screen conditions and transduced Gesicle cells with a lentiviral
111 vector encoding constitutive expression of Cas9 nuclease and an appropriate targeting
112 sgRNA, selected cells for Cas9 expression, and isolated a polyclonal population of Cas9-
113 edited cells (Extended Data Fig. 2a). To control for the effects of Cas9 expression and
114 Cas9 nuclease-mediated indel generation on producer cells, we also applied the same
115 procedure to generate modified Gesicle cells using a sgRNA targeting *AAVS1*, a human
116 safe harbor locus[28]. After knockout generation, we initiated v4 BE-eVLP production from

117 each cell line by transfecting plasmids encoding the expression of all required
118 components, including a sgRNA targeting the human *BCL11A* +58 enhancer locus[29]
119 (Extended Data Fig. 2a). We detected by RT-qPCR a 1.5- to 3.8-fold decrease in sgRNA
120 abundance in BE-eVLPs produced from HUSH-knockout cells compared to BE-eVLPs
121 produced from *AAVS1*-knockout cells (Fig. 1c), confirming the results of our screen.
122 Additionally, when we transduced HEK293T cells with a range of doses of purified BE-
123 eVLPs and measured adenine base editing efficiencies at the *BCL11A* +58 enhancer
124 target locus via high-throughput sequencing (Extended Data Fig. 2a), we observed that
125 BE-eVLPs produced from HUSH-knockout cells exhibited a 2.3- to 4.4-fold decrease in
126 *in vitro* delivery potency (EC_{50}) compared to BE-eVLPs produced from *AAVS1*-knockout
127 cells (Fig. 2d). These results indicate that knockout of HUSH-associated genes *MPP8*,
128 *TASOR*, or *MORC2* in producer cells negatively impacts eVLP production or cargo
129 loading.

130 We hypothesized that these HUSH-associated genes might impact eVLP
131 production or cargo loading by modulating the expression of the lentivirally integrated
132 Cas9 nuclease that was used to generate the gene knockouts. To test this hypothesis,
133 we measured the relative abundance of Cas9 mRNA or protein in each knockout cell line
134 by RT-qPCR or Western blot respectively. We observed a 5.4- to 29-fold increase in
135 cellular Cas9 mRNA expression and a 10- to 14-fold increase in Cas9 protein expression
136 in HUSH-knockout cells compared to *AAVS1*-knockout cells (Fig. 1e, f and Extended Data
137 Fig. 3a). These results suggest a model in which HUSH-associated gene products
138 natively silence lentivirally integrated Cas9 expression in *AAVS1*-knockout producer cells,
139 but in HUSH-knockout cells, Cas9 is no longer efficiently silenced (Extended Data Fig.
140 3b). Therefore, during eVLP production, excess Cas9 protein in HUSH-knockout producer
141 cells likely competes for sgRNA binding and prevents sgRNA molecules from efficiently
142 binding to gag–ABE, which ultimately decreases both sgRNA packaging into eVLPs and
143 eVLP delivery potency (Extended Data Fig. 3b). To further investigate this phenomenon,
144 we used v4 Cas9-eVLP transduction instead of Cas9/sgRNA lentiviral transduction to
145 generate HUSH-knockout Gesicle cells that lacked any integrated Cas9 transgene
146 (Extended Data Fig. 2b). Notably, we did not detect any change in sgRNA abundance by
147 RT-qPCR in BE-eVLPs produced from these Cas9-free HUSH-knockout cells compared

148 to standard producer cells (Extended Data Fig. 4a). These results suggest that, consistent
149 with our model above, both lentivirally integrated Cas9 expression and knockout of
150 HUSH-associated genes are required to decrease sgRNA abundance in eVLPs.
151 Collectively, these data and our proposed model rationalize the negative performance of
152 HUSH-associated gene knockouts in our screen.

153 Interestingly, we noticed that BE-eVLPs produced from Cas9-free HUSH-knockout
154 cells still exhibited a 2.6- to 3.9-fold decrease in delivery potency compared to BE-eVLPs
155 produced from standard Gesicle cells (Extended Data Fig. 4b), suggesting that some
156 eVLP property other than sgRNA abundance was negatively impacted due to Cas9-free
157 HUSH-associated gene knockout. We hypothesized that these HUSH-associated genes
158 might also modulate the expression of eVLP components from plasmids transfected
159 during the eVLP production process. To investigate this possibility, we performed
160 Western blots to quantify eVLP cargo (gag–ABE) expression in producer cells following
161 transfection of eVLP production plasmids, which revealed a 2.1- to 4.4-fold increase in
162 gag–ABE protein expression in HUSH-knockout cells compared to Gesicle cells
163 (Extended Data Fig. 4c, d). We reasoned that this increase in eVLP cargo expression
164 might disrupt the optimal eVLP component stoichiometry (gag–ABE:gag–pro–pol ratio),
165 which was previously found to be an important determinant of eVLP potency[8]. Indeed,
166 reducing the transfected gag–ABE:gag–pro–pol plasmid ratio from 25:75 to 10:90 or 5:95
167 restored the potency of BE-eVLPs produced from *MORC2*-knockout cells back to
168 standard levels (Extended Data Fig. 4e). These results indicate that the increase in eVLP
169 cargo expression in HUSH-knockout producer cells and corresponding disruption of the
170 optimal eVLP component stoichiometry can be counteracted simply by reducing the
171 amount of transfected eVLP cargo plasmid, thereby effectively restoring the optimal
172 stoichiometry. Altogether, our results reveal a previously unknown role for HUSH-
173 associated genes in modulating eVLP cargo expression in producer cells and highlight
174 the importance of optimizing eVLP cargo expression and component stoichiometry to
175 maximize eVLP potency.

176 Next, we sought to characterize the gene knockouts from our screen that most
177 strongly increased eVLP production or cargo loading. The single strongest positive hit
178 from our screen was *MAF1*, a repressor of RNA Pol III transcription[30-32]. Because all

179 sgRNAs in our experiments were expressed from an RNA Pol III-transcribed U6 promoter,
180 we reasoned that knockout of *MAF1* in producer cells likely leads to increased sgRNA
181 transcription and loading into eVLP-packaged cargos (Fig. 2a). To test this hypothesis,
182 after generating *MAF1*-knockout Gesicle cells using v4 Cas9-eVLPs (Extended Data Fig.
183 2b), we initiated v4 BE-eVLP production from these cells by transfecting plasmids
184 encoding the expression of all required components. We detected by RT-qPCR a 2-fold
185 increase in sgRNA abundance in BE-eVLPs produced from *MAF1*-knockout cells
186 compared to BE-eVLPs produced from standard Gesicle cells (Fig. 2b). Additionally, we
187 observed that BE-eVLPs produced from *MAF1*-knockout cells were produced at similar
188 particle titers and packaged similar numbers of BE cargo proteins per particle compared
189 to BE-eVLPs produced from standard Gesicle cells (Fig. 2c and Extended Data Fig. 5a),
190 suggesting that the use of *MAF1*-knockout cells increases sgRNA packaging alone
191 without affecting protein packaging or particle yield. Collectively, these data confirm our
192 knockout screen results and indicate that *MAF1*-knockout producer cells support
193 increased sgRNA loading into eVLPs.

194 Because increased sgRNA loading leads to an increased number of active RNP
195 cargo molecules packaged into eVLPs (Fig. 2a), we reasoned that BE-eVLPs produced
196 from *MAF1*-knockout cells should exhibit increased delivery potency compared to BE-
197 eVLPs produced from standard Gesicle cells. Encouragingly, we observed that v4 BE-
198 eVLPs produced from *MAF1*-knockout cells exhibited a 2.5-fold increase in delivery
199 potency (EC_{50}) at the *BCL11A* +58 enhancer locus in HEK293T cells compared to v4 BE-
200 eVLPs produced from standard Gesicle cells (Fig. 2d). v4 BE-eVLPs produced from
201 *MAF1*-knockout cells also exhibited a 2.2- and 2.1-fold increase in delivery potency at the
202 *GAPDH* and *HIRA* genomic loci in HEK293T cells, respectively (Fig. 2e, f), indicating that
203 the eVLP potency improvement conferred by the use of *MAF1*-knockout producer cells is
204 not restricted to any particular sgRNA sequence or target genomic locus. Additionally, we
205 assessed whether the use of *MAF1*-knockout producer cells could also improve the
206 delivery potency of the more recently developed v5 BE-eVLPs, which use laboratory
207 evolved capsid proteins that were optimized to improve BE RNP cargo packaging[22]. We
208 observed that v5 BE-eVLPs produced from *MAF1*-knockout cells exhibited a 2.2- to 9.1-
209 fold increase in delivery potency compared to v5 BE-eVLPs produced from standard cells

210 across six distinct target genomic loci in mouse Neuro-2a cells (Fig. 2g–l). Together,
211 these results indicate that the increased sgRNA packaging in BE-eVLPs produced from
212 *MAF1*-knockout cells leads to corresponding improvements in eVLP delivery potency *in*
213 *vitro*.

214 To further explore the utility of *MAF1*-knockout producer cells, we investigated
215 whether their use could also improve *in vivo* eVLP delivery efficiencies. We produced v5
216 BE-eVLPs targeting the *Pcsk9* exon 1 splice donor[8,33] using either standard or *MAF1*-
217 knockout Gesicle cells, and we injected these BE-eVLPs retro-orbitally into adult mice at
218 a low, sub-saturating eVLP dose (Fig. 2m). We observed that v5 BE-eVLPs produced
219 from *MAF1*-knockout cells achieved 19.4% average *in vivo* base editing at the *Pcsk9*
220 locus in bulk liver tissue, while v5 BE-eVLPs produced from standard cells administered
221 at the same dose only achieved 12.6% bulk liver editing (Fig. 2m, $P = 0.0365$, two-sided
222 unpaired *t* test). Collectively, these data indicate that *MAF1*-knockout producer cells
223 support improved eVLP potency across different target genomic loci and target-cell types
224 both *in vitro* and *in vivo*, demonstrating the benefits of using *MAF1*-knockout cells instead
225 of standard cells for eVLP production.

226 We next sought to further evaluate the ability of *MAF1*-knockout producer cells to
227 support improved eVLP production and potency in other various contexts. First, we
228 assessed whether *MAF1*-knockout producer cells could improve the potency of eVLPs
229 that package different Cas9-based RNP cargos. We observed that v4 eVLPs packaging
230 either ABE8e-SpCas9-NG[34], TadCBEa[35], or Cas9 nuclease cargos exhibited a 2.0- to
231 2.5-fold improvement in potency in HEK293T cells when produced from *MAF1*-knockout
232 cells compared to Gesicle cells (Extended Data Fig. 5b–f). Second, we investigated
233 whether *MAF1*-knockout producer cells could also improve the performance of non-eVLP
234 delivery vehicles, such as the recently reported "engineered nucleocytosolic vehicles for
235 loading of programmable editors" (ENVLPE$^+$)[10]. Interestingly, we observed that ABE8e-
236 packaging ENVLPE$^+$ particles produced from *MAF1*-knockout cells also exhibited a 2.2-
237 fold increase in potency in HEK293T cells compared to the same particles produced from
238 Gesicle cells (Extended Data Fig. 5g). Notably, even though ENVLPE$^+$ particles differ
239 substantially from eVLPs in their viral scaffold (HIV versus MMLV) and cargo loading
240 mechanism (aptamer-containing sgRNA loading versus gag–cargo fusion loading), both

241 ENVLPE^{+} particles and eVLPs demonstrated nearly identical improvements in potency
242 when produced from *MAF1*-knockout cells compared to Gesicle cells (Extended Data Fig.
243 5g, h). Third, we explored whether knockout of *MAF1* could improve eVLP production
244 from HEK293T/17 cells, another cell line that is commonly used for viral vector
245 production[8,22,36]. Following the generation of *MAF1*-knockout HEK293T/17 cells using v4
246 Cas9-eVLPs, we observed that v4 BE-eVLPs produced from *MAF1*-knockout
247 HEK293T/17 cells exhibited a 2.5-fold increase in *in vitro* delivery potency compared to
248 those produced from unmodified HEK293T/17 cells (Fig. 2n). These results indicate that
249 the improvements conferred by *MAF1* knockout appear to be generalizable beyond the
250 specific cell line in which our knockout screen was conducted. Taken together, our
251 findings demonstrate that knockout of *MAF1* in producer cells yields remarkably general
252 and consistent improvements in VLP delivery potency across eVLP cargo types, particle
253 types, and producer-cell lines.

254 We anticipate that the use of *MAF1*-knockout cells instead of standard producer
255 cells will advance the utility of VLP delivery in several ways. For one, eVLPs produced
256 from *MAF1*-knockout cells exhibit increased sgRNA packaging and increased delivery
257 potency both in cell culture and in mice compared to standard eVLPs (Fig. 2), suggesting
258 that *MAF1*-knockout producer cells should be used when maximal editing efficiencies are
259 required. Additionally, the gene editing efficiencies at a given dose of eVLPs produced
260 from standard cells can in general be achieved using a 2- to 9-fold lower dose of eVLPs
261 produced from *MAF1*-knockout cells (Fig. 2d–l), suggesting that using *MAF1*-knockout
262 cells for eVLP production will be especially beneficial for applications that are constrained
263 by the maximum administrable eVLP dose. Furthermore, by minimizing the eVLP dose
264 required to achieve efficient editing, the use of *MAF1*-knockout producer cells would also
265 reduce the total volume of producer-cell culture required for eVLP production, which could
266 greatly simplify the application of eVLPs in large-scale studies. Importantly, given that
267 several previous studies have identified sgRNA loading into VLPs and related delivery
268 vehicles as a bottleneck that limits delivery potency[8,13,22,37], our discovery that *MAF1*-
269 knockout producer cells improve sgRNA loading into VLPs will likely be widely applicable
270 for RNP delivery using various cell-derived bioparticles.

271 Altogether, our study provides a general workflow for genetically engineering
272 producer cells for improved particle production. By applying a genome-wide knockout
273 screen to nominate genetic perturbations that influence eVLP production, we discovered
274 that several genes regulate protein and sgRNA expression in producer cells, both of
275 which proved to strongly impact eVLP cargo packaging and delivery potency. While
276 previous studies have applied CRISPR screens that use particle-packaged RNA as a way
277 to investigate the cellular determinants of extracellular vesicle production[38,39], our study
278 is the first to our knowledge that leverages insights from a producer-cell screen to improve
279 VLP production and delivery potency. Notably, our screen design is highly general and
280 can be applied to evaluate various genetic and epigenetic perturbations on a genome-
281 wide scale, including for CRISPR activation or base editing screens. We anticipate that
282 further improvements in particle production are likely possible by employing varied
283 producer-cell perturbations instead of single gene knockouts alone. Overall, while
284 iterative particle architecture engineering continues to improve VLP delivery potency and
285 cell-type targeting capabilities[10,13,22,40], our work establishes producer-cell genetic
286 engineering as a distinct and potentially powerful strategy for maximizing the utility of
287 VLP-based delivery modalities.

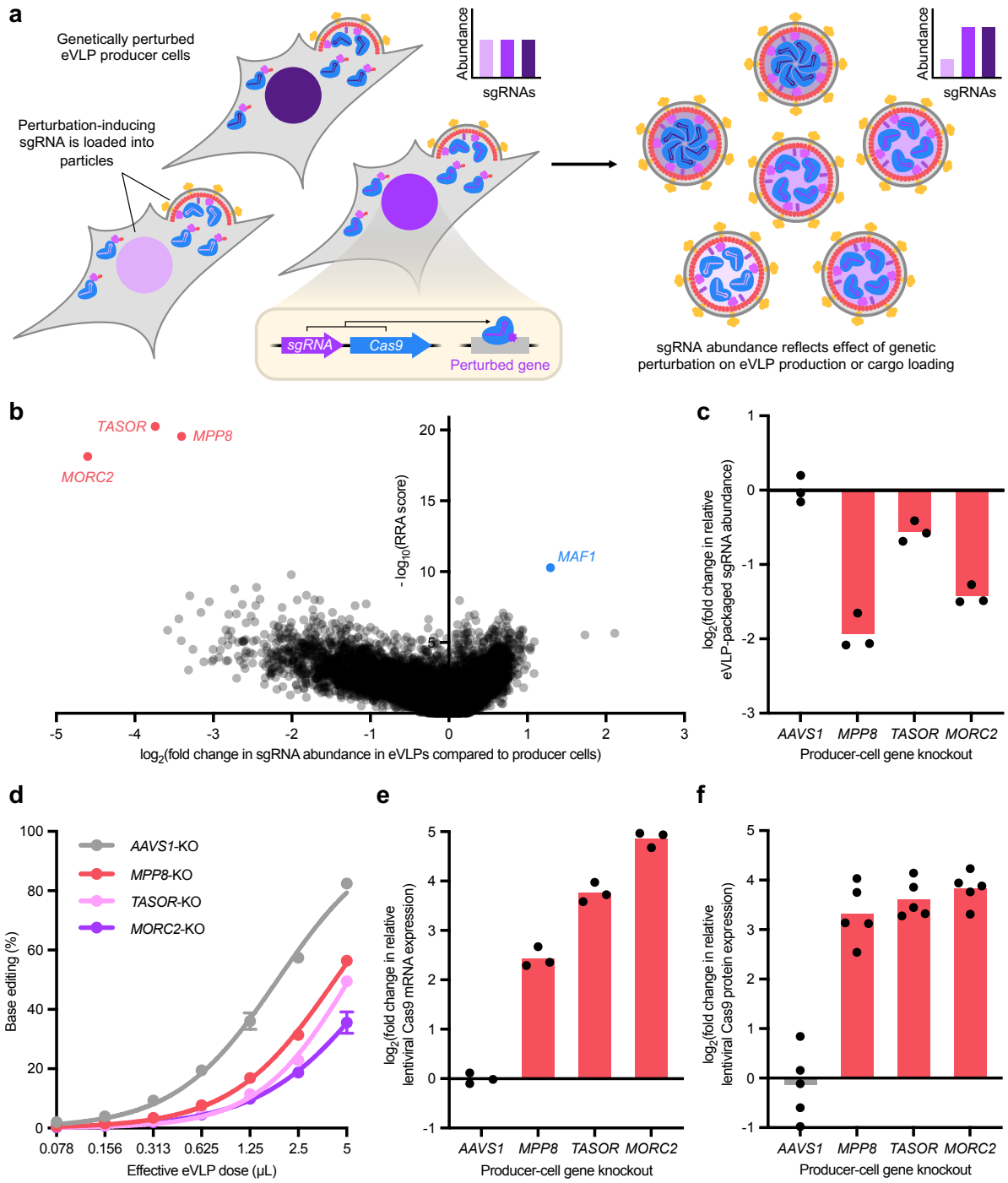

Fig. 1 | Genome-wide screening reveals genetic perturbations that influence eVLP production. a, Overview of the producer-cell screening approach. eVLP production is initiated from a pool of genetically perturbed producer cells, and each eVLP packages sgRNAs that identify the specific genetic perturbation in the cell that produced that particular eVLP. The abundance of a particular sgRNA in eVLPs compared to producer cells reflects how the corresponding genetic perturbation influences eVLP production or cargo loading. **b**, Gene-level phenotypes from the genome-wide knockout screen for cargo-loaded eVLP production. Each gene is represented as a single dot whose x-

297 coordinate reflects the median fold change in sgRNA abundance in eVLPs compared to
298 producer cells for all sgRNAs targeting that particular gene, and whose y-coordinate
299 reflects the MAGeCK RRA score associated with that particular gene (see Methods). Data
300 reflect n=2 screen replicates. See also Extended Data Fig. 1c and Supplementary Table
301 6. **c**, Fold change in eVLP-packaged sgRNA abundance measured by RT-qPCR,
302 normalized relative to sgRNA abundance in eVLPs produced from *AAVS1*-knockout cells.
303 Bars reflect the mean of n=3 replicates, and dots represent individual replicate values. **d**,
304 Comparison of v4 BE-eVLPs produced from *AAVS1*-knockout or HUSH-knockout cells
305 across a range of eVLP doses. Adenine base editing efficiencies at position A_7 of the
306 *BCL11A* +58 enhancer site in HEK293T cells are shown. Dots and error bars represent
307 mean ± s.d. of n=3 biological replicates. Data were fit to four-parameter logistic curves
308 using nonlinear regression. **e**, Fold change in producer-cell Cas9 mRNA abundance
309 measured by RT-qPCR, normalized relative to Cas9 mRNA abundance in *AAVS1*-
310 knockout cells. Bars reflect the mean of n=3 replicates, and dots represent individual
311 replicate values. **f**, Fold change in producer-cell Cas9 protein abundance measured by
312 Western blot, normalized relative to Cas9 protein abundance in *AAVS1*-knockout cells.
313 Bars reflect the mean of n=5 replicates, and dots represent individual replicate values.
314 See also Extended Data Fig. 3a.

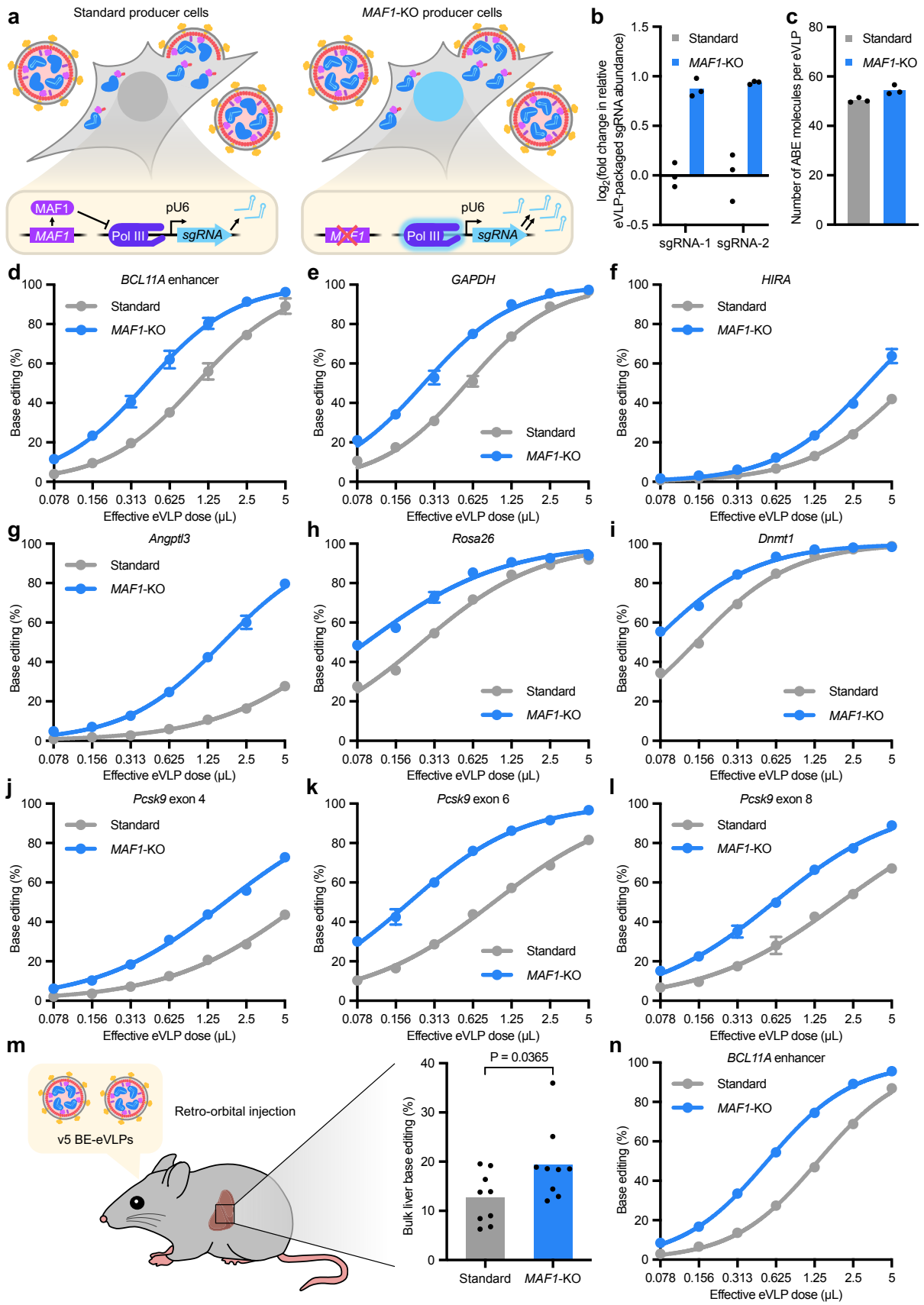
a
Standard producer cells
MAF1-KO producer cells
MAF1
MAF1
Pol III
pU6
sgRNA
b
log2(fold change in relative eVLP-packaged sgRNA abundance)
Standard
MAF1-KO
sgRNA-1
sgRNA-2
c
Number of ABE molecules per eVLP
d
BCL11A enhancer
e
GAPDH
f
HIRA
g
Angptl3
h
Rosa26
i
Dnmt1
j
Pcsk9 exon 4
k
Pcsk9 exon 6
l
Pcsk9 exon 8
Base editing (%)
Effective eVLP dose (μL)
m
v5 BE-eVLPs
Retro-orbital injection
P = 0.0365
Bulk liver base editing (%)
n

Fig. 2 | *MAF1*-knockout producer cells improve eVLP sgRNA packaging and delivery potency. a, Schematic of standard producer cells versus *MAF1*-knockout producer cells. In standard cells, MAF1 represses RNA Pol III transcription, which limits producer-cell sgRNA expression. In *MAF1*-knockout producer cells, RNA Pol III is no longer subjected to MAF1-mediated repression, which increases sgRNA expression and loading into eVLP-packaged RNPs. **b**, Fold change in eVLP-packaged sgRNA abundance measured by RT-qPCR, normalized relative to sgRNA abundance in eVLPs produced from standard Gesicle cells. sgRNA-1 and sgRNA-2 denote two different packaged sgRNA sequences. **c**, Quantification of ABE molecules per eVLP by anti-Cas9 and anti-MLV p30 ELISA. In **b** and **c**, bars reflect the mean of n=3 replicates, and dots represent individual replicate values. **d–f**, Comparison of v4 BE-eVLPs produced from standard or *MAF1*-knockout Gesicle cells across a range of eVLP doses in HEK293T cells. Adenine base editing efficiencies are shown at position A_7 of the *BCL11A* +58 enhancer site (**d**), position A_7 of the *GAPDH* site (**e**), and position A_5 of the *HIRA* site (**f**). **g–l**, Comparison of v5 BE-eVLPs produced from standard or *MAF1*-knockout Gesicle cells across a range of eVLP doses in mouse Neuro-2a cells. Adenine base editing efficiencies are shown at position A_8 of the *Angptl3* exon 7 splice acceptor site (**g**), position A_4 of the *Rosa26* site (**h**), position A_9 of the *Dnmt1* site (**i**), position A_6 of the *Pcsk9* exon 4 splice acceptor site (**j**), position A_4 of the *Pcsk9* exon 6 splice donor site (**k**), and position A_8 of the *Pcsk9* exon 8 splice acceptor site (**l**). **m**, Schematic of mouse experiments and adenine base editing efficiencies at position A_6 of the *Pcsk9* exon 1 splice donor site in bulk mouse liver tissue. Each mouse was injected with 15 µL of 1500-fold concentrated purified eVLPs, corresponding to approximately 3×10^{11} eVLPs (see Methods). Bars reflect the mean of n=9 mice per condition, and dots represent individual mouse values. P-value was calculated using a two-sided unpaired t test. **n**, Comparison of v4 BE-eVLPs produced from standard or *MAF1*-knockout HEK293T/17 cells across a range of eVLP doses in HEK293T cells. Adenine base editing efficiencies at position A_7 of the *BCL11A* +58 enhancer site are shown. In **d–l** and **n**, dots and error bars represent mean ± s.d. of n=4 (**d**) or n=3 (**e–l**, **n**) biological replicates. Data were fit to four-parameter logistic curves using nonlinear regression.

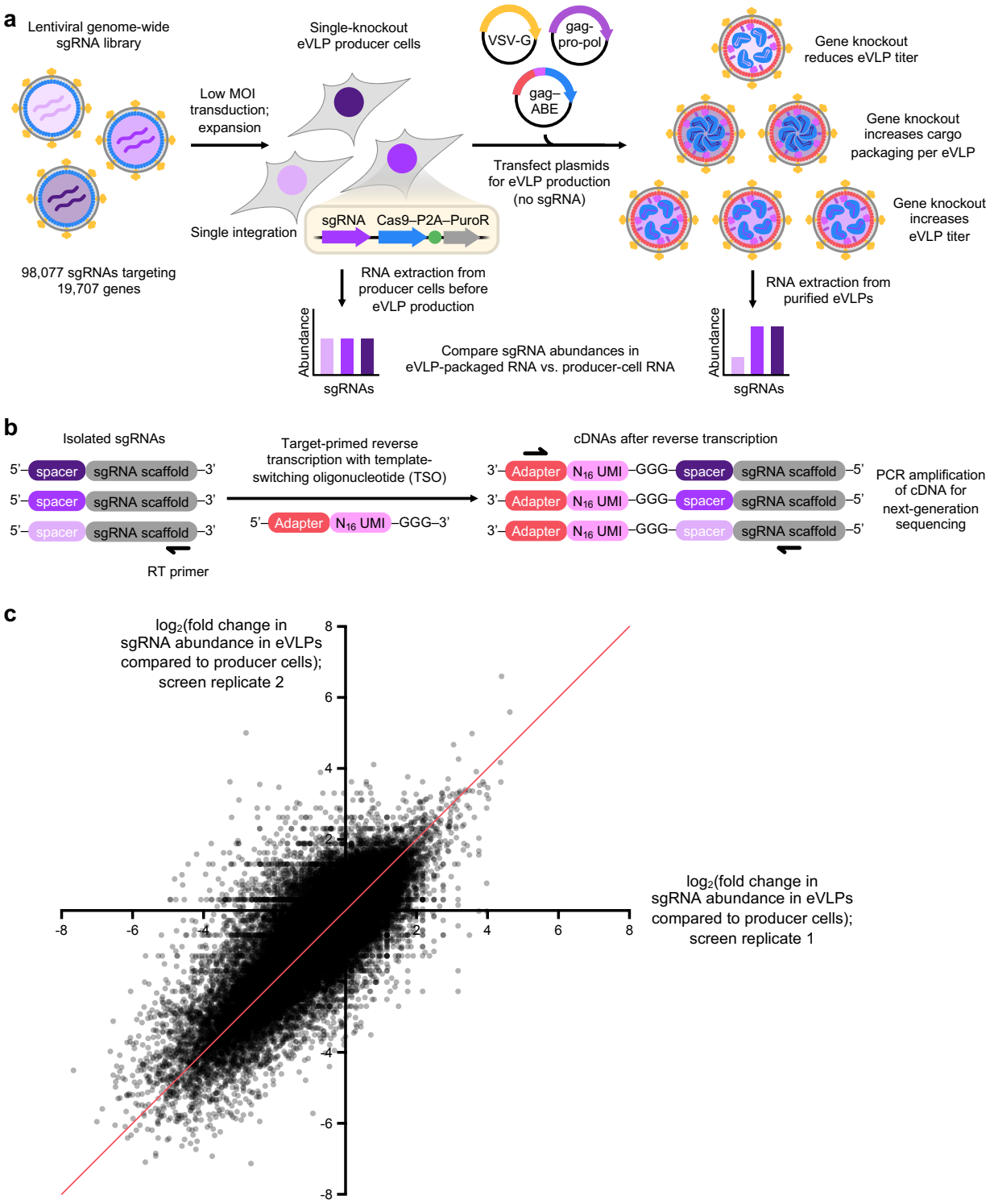

Extended Data Fig. 1 | Genome-wide knockout screening for cargo-loaded eVLP production. a, Overview of the genome-wide knockout screening approach. Low-MOI Cas9/sgRNA lentiviral transduction was used to introduce a genome-wide sgRNA library into Gesicle producer cells, thereby generating a pool of single-knockout producer cells. eVLP production was then initiated from this pool by transfecting expressing eVLP protein

352 components. No additional sgRNA-encoding plasmid was transfected, ensuring that all
353 eVLPs produced from a given producer cell packaged cargo containing the specific
354 knockout-inducing sgRNA that was already introduced into that producer cell by lentiviral
355 transduction. The abundance of a particular sgRNA in eVLPs compared to producer cells
356 reflects how the corresponding gene knockout influences eVLP production or cargo
357 loading. **b**, Schematic of the template-switching reverse transcription approach used for
358 direct-capture sgRNA spacer sequencing from both eVLP-packaged RNA and producer-
359 cell RNA. UMI=unique molecular identifier. **c**, Fold change in sgRNA abundance in eVLPs
360 compared to producer cells across replicates of the genome-wide knockout screen. Each
361 sgRNA in the library is represented as a single dot and reflects the values from n=2 screen
362 replicates. The y=x line is plotted in red. See also Supplementary Tables 3–5.

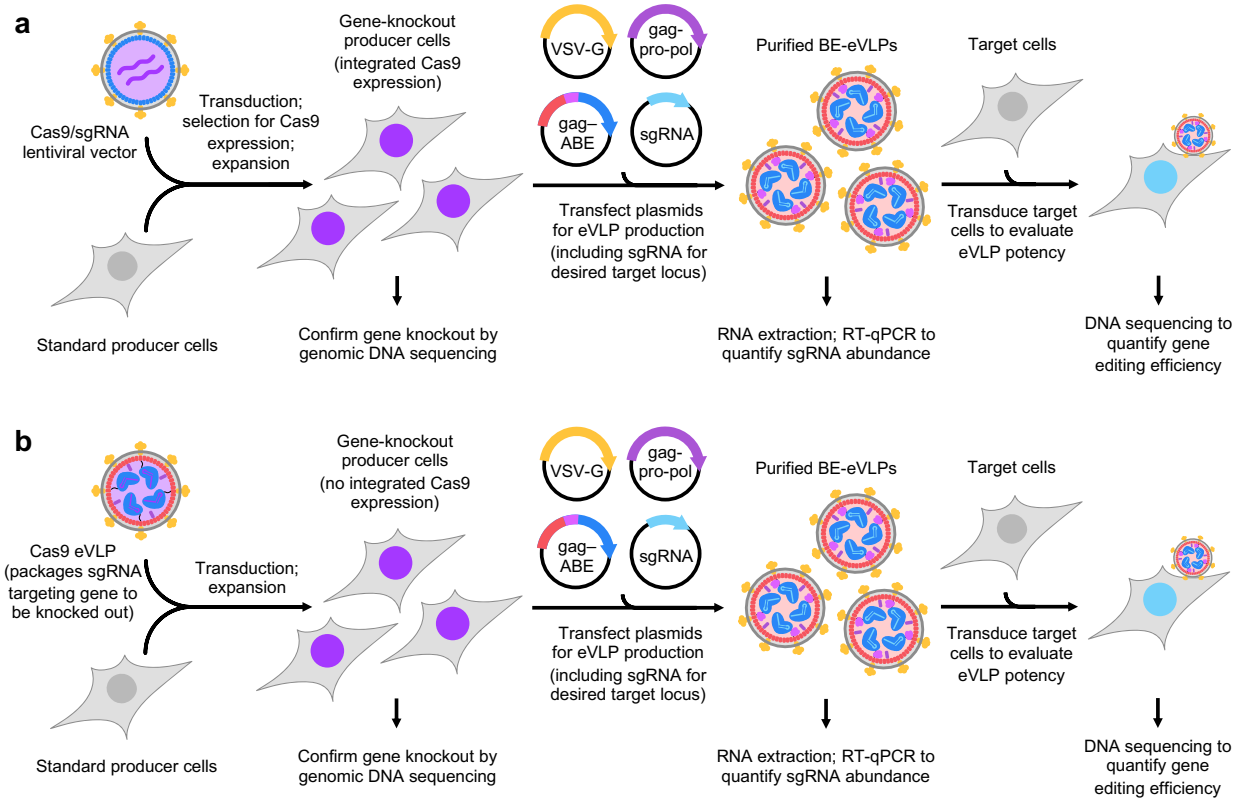

Extended Data Fig. 2 | Generating and characterizing single-knockout producer cell lines. a, Schematic of generating polyclonal single-knockout producer cells via Cas9/sgRNA lentiviral transduction, followed by characterizing the resulting cell lines and their use for eVLP production. **b**, Schematic of generating polyclonal single-knockout producer cells via v4 Cas9-eVLP transduction, followed by characterizing the resulting cell lines and their use for eVLP production.

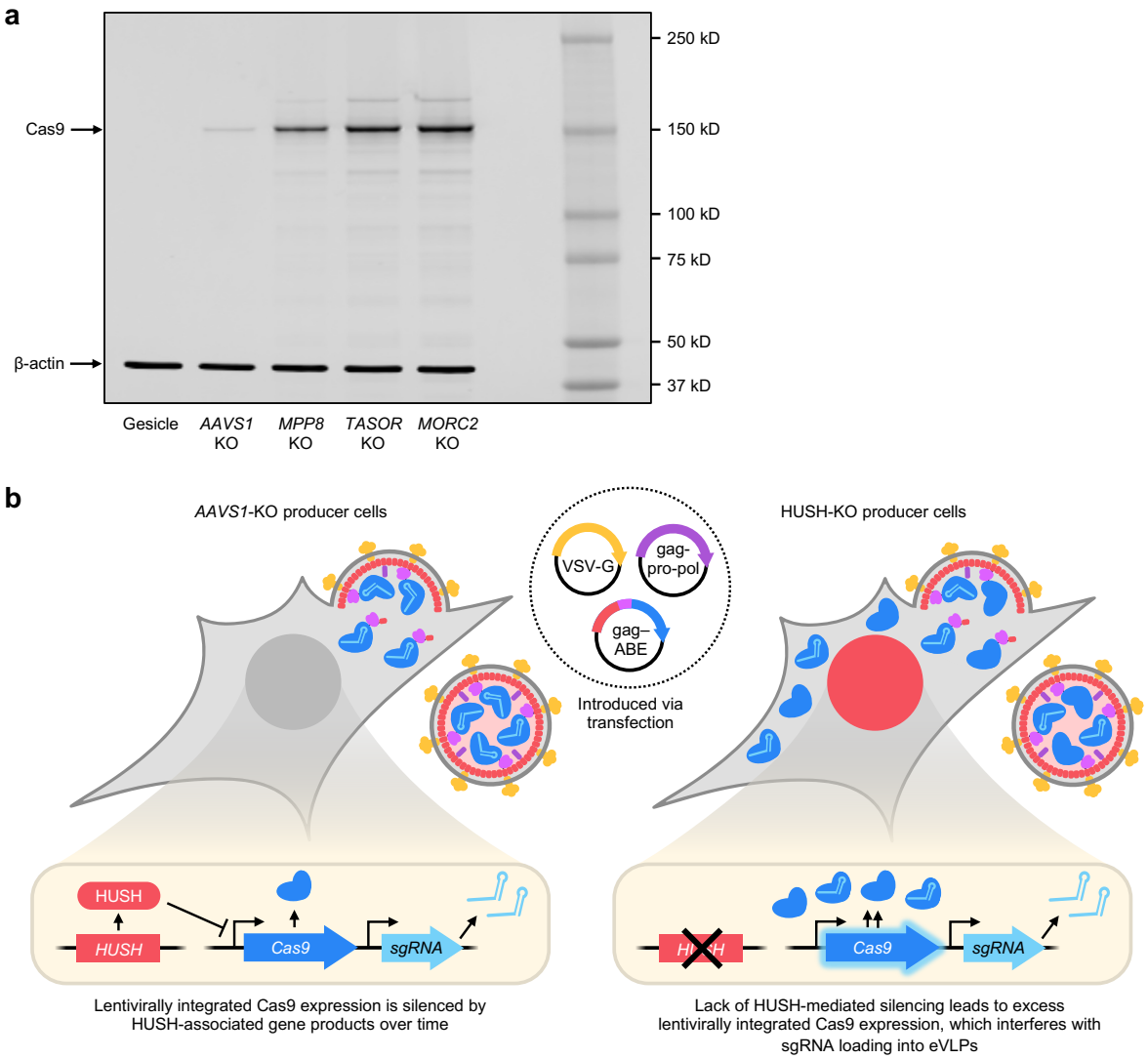

Extended Data Fig. 3 | HUSH-knockout producer cells exhibit increased lentiviral Cas9 expression. a, Western blot analysis of producer-cell protein lysates. **b**, Proposed model for *AAVS1*-knockout producer cells versus HUSH-knockout producer cells. In *AAVS1*-knockout cells, HUSH-associated gene products silence lentivirally integrated Cas9 expression over time. In HUSH-knockout producer cells, lack of HUSH-mediated silencing leads to excess expression of lentivirally integrated Cas9, which interferes with sgRNA loading into eVLPs and therefore reduces eVLP-packaged sgRNA abundance.

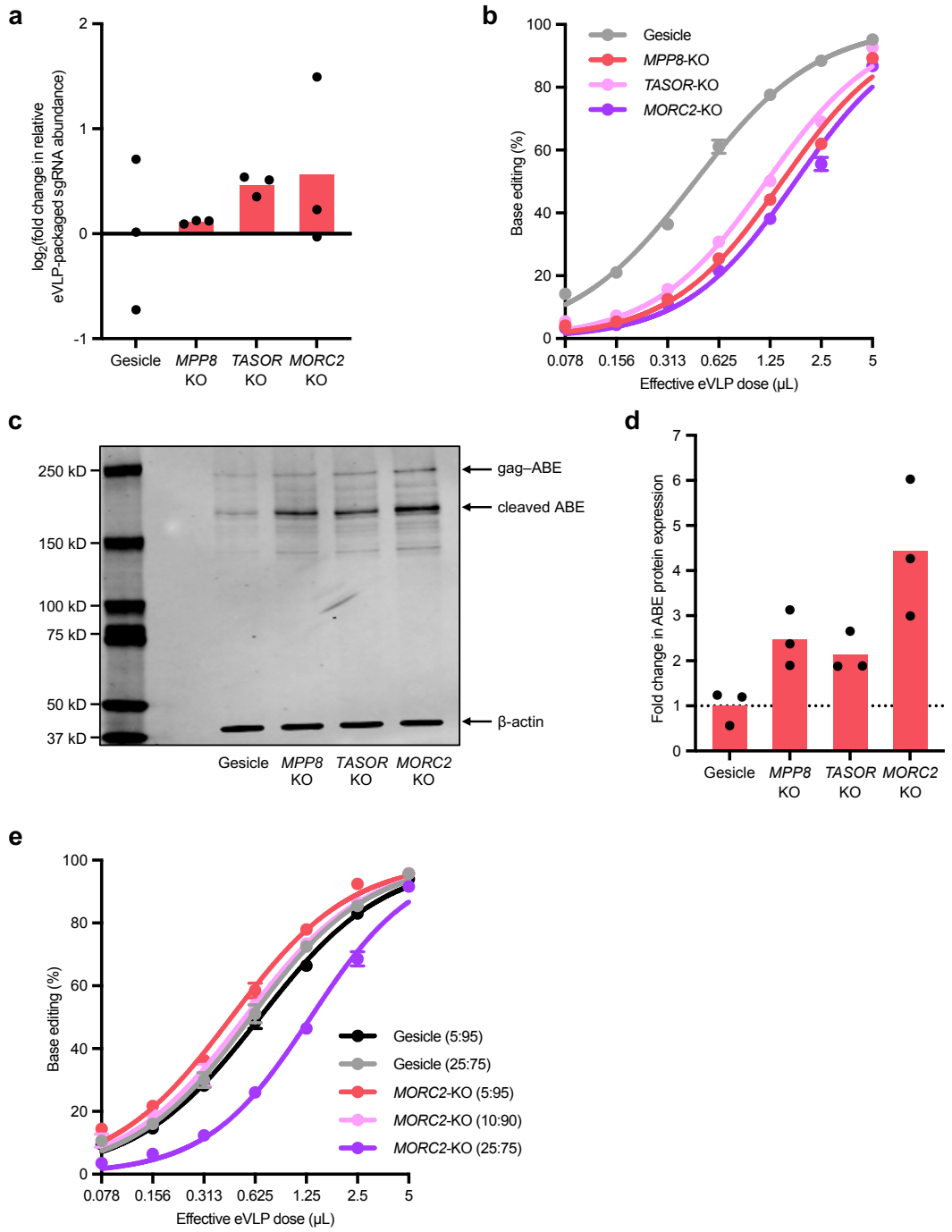

Extended Data Fig. 4 | HUSH-knockout producer cells exhibit increased eVLP cargo expression. a, Fold change in eVLP-packaged sgRNA abundance measured by RT-qPCR, normalized relative to sgRNA abundance in eVLPs produced from Gesicle cells. Bars reflect the mean of n=3 replicates, and dots represent individual replicate values. **b**, Comparison of v4 BE-eVLPs produced from Gesicle or HUSH-knockout cells across a range of eVLP doses. Adenine base editing efficiencies at position A_7 of the *BCL11A* +58 enhancer site in HEK293T cells are shown. Dots and error bars represent mean ± s.d. of n=3 biological replicates. Data were fit to four-parameter logistic curves using nonlinear

regression. **c**, Western blot analysis of protein lysates from producer cells transfected with eVLP production plasmids. The full-length gag–ABE fusion is ~247 kD and the cleaved ABE (following viral protease-mediated cleavage) is ~184 kD. **d**, Fold change in transfected-producer-cell ABE protein abundance measured by Western blot, normalized relative to ABE protein abundance in transfected Gesicle cells. Bars reflect the mean of n=3 replicates, and dots represent individual replicate values. **e**, Comparison of v4 BE-eVLPs produced from Gesicle or *MORC2*-knockout cells across a range of eVLP doses using different transfected eVLP plasmid stoichiometries. Values in parentheses reflect the gag–ABE:gag–pro–pol plasmid ratio used for eVLP production. Adenine base editing efficiencies at position A_7 of the *BCL11A* +58 enhancer site in HEK293T cells are shown. Dots and error bars represent mean ± s.d. of n=3 biological replicates. Data were fit to four-parameter logistic curves using nonlinear regression.

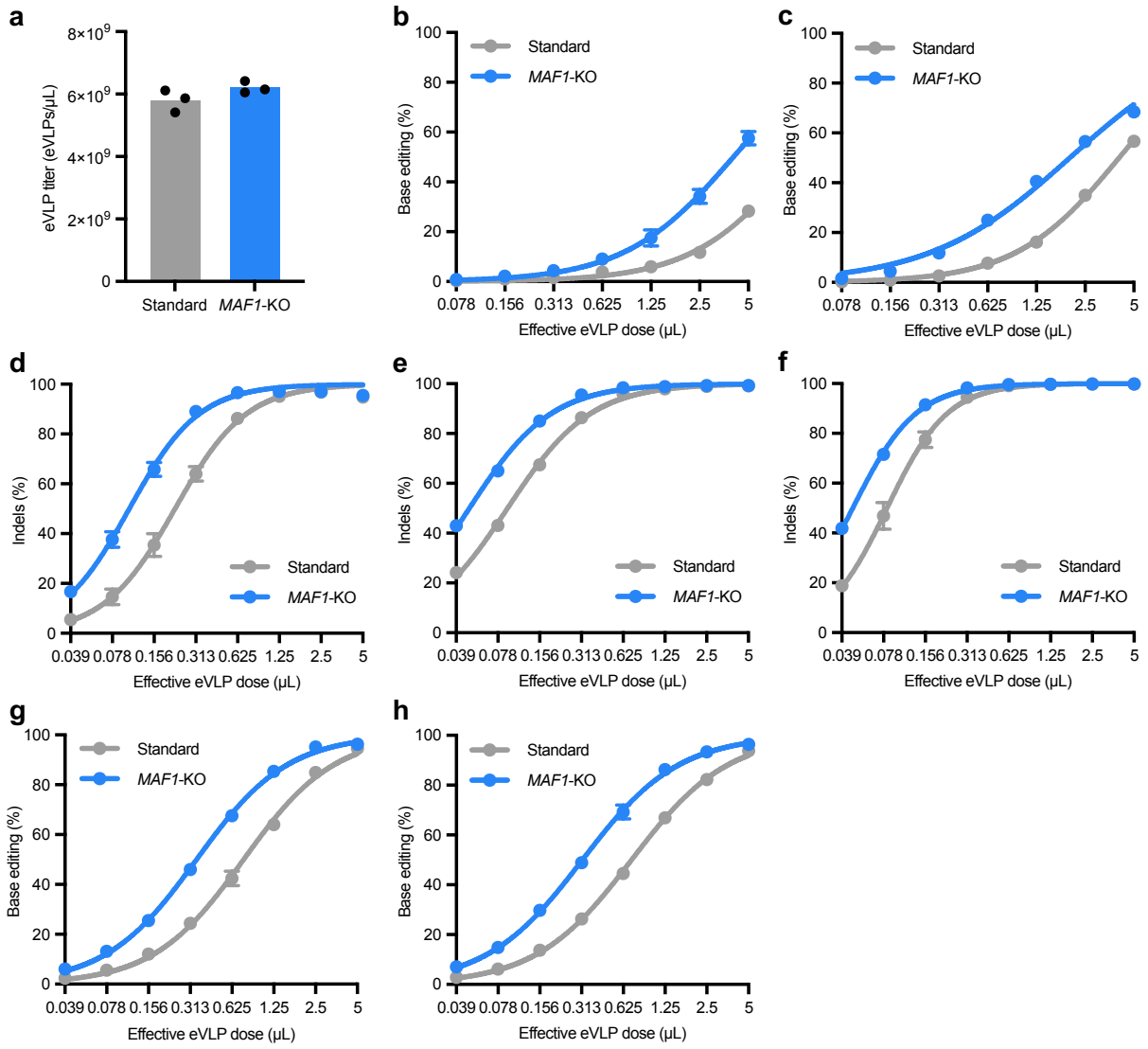

Extended Data Fig. 5 | *MAF1*-knockout producer cells improve eVLP delivery potency. a, Quantification of eVLP titer by anti-MLV p30 ELISA (see Methods). Bars reflect the mean of n=3 replicates, and dots represent individual replicate values. **b**, Comparison of v4 ABE8e-NG-eVLPs produced from standard or *MAF1*-knockout Gesicle cells across a range of eVLP doses. Adenine base editing efficiencies at position A_7 of the *BCL11A* +58 enhancer site in HEK293T cells are shown. **c**, Comparison of v4 TadCBEa-eVLPs produced from standard or *MAF1*-knockout Gesicle cells across a range of eVLP doses. Cytosine base editing efficiencies at position C_6 of the *BCL11A* +58 enhancer site in HEK293T cells are shown. **d–f**, Comparison of v4 Cas9-eVLPs produced from standard or *MAF1*-knockout Gesicle cells across a range of eVLP doses in HEK293T cells. Indel frequencies are shown at the *BCL11A* +58 enhancer site (**d**), *HEK2* site (**e**), and *EMX1* site (**f**). **g–h**, Comparison of ABE8e-packaging ENVLPE$^+$ particles (**g**) or v4 ABE8e-eVLPs (**h**) produced from standard or *MAF1*-knockout Gesicle cells across a range of doses. Adenine base editing efficiencies at position A_7 of the *BCL11A* +58 enhancer site in HEK293T cells are shown. **b–h**, Dots and error bars represent mean ±

415 s.d. of n=3 biological replicates. Data were fit to four-parameter logistic curves using
416 nonlinear regression.
417

418 **Methods**
419
420 **Cloning**
421 Plasmids used in this study were cloned via Gibson cloning (NEBuilder® HiFi DNA
422 Assembly; E2621X) or Golden Gate cloning. DNA was amplified via PCR using Phusion
423 HotStart II polymerase (Thermo Fisher Scientific; F537L). Mach1 (Thermo Fisher
424 Scientific; C862003) or NEB® Stable (New England Biolabs; C3040H) chemically
425 competent *E. coli* were used for plasmid propagation. Plasmids were isolated using
426 QIAGEN Plasmid Plus Midi (12945) or Maxi (12963) Kits according to the manufacturer's
427 protocols.
428
429 **Cell culture**
430 HEK293T cells (ATCC; CRL-3216), Gesicle Producer 293T cells (Takara; 632617),
431 HEK293T/17 cells (ATCC; CRL-11268), and Neuro-2a cells (ATCC; CCL-131) were
432 maintained in DMEM + GlutaMAX (Life Technologies; 10569044) supplemented with 10%
433 (v/v) fetal bovine serum (Gibco; A5670701). Cells were cultured at 37 °C with 5% carbon
434 dioxide and were confirmed to be negative for mycoplasma by testing with MycoAlert
435 (Lonza; LT07-318).
436
437 **eVLP production and purification**
438 eVLPs were produced as described previously[8,22]. Briefly, eVLPs were produced by
439 transient transfection of Gesicle 293T cells, HEK293T/17 cells, or variants thereof as
440 noted in the main text and figure legends. Producer cells were seeded in T-75 flasks at a
441 density of 5×10^6 cells per flask. After 20–24 h, cells were transfected using the jetPRIME
442 transfection reagent (Polyplus; 114-75) according to the manufacturer's protocols. For
443 producing eVLPs, a mixture of plasmids expressing VSV-G (400 ng), MMLV gag-pro-pol
444 (3,375 ng), gag–cargo (1,125 ng), and an sgRNA (4,400 ng) was co-transfected per T-75
445 flask.
446 40–48 h post-transfection, producer cell supernatant was harvested and
447 centrifuged for 5 min at 500 g to remove cell debris. The clarified eVLP-containing
448 supernatant was filtered through a 0.45-µm PVDF filter (Millipore; SE1M003M00). The
449 filtered supernatant was concentrated 100-fold using PEG-it Virus Precipitation Solution
450 (System Biosciences; LV825A-1) according to the manufacturer's protocols and
451 resuspended in Opti-MEM serum-free media (Thermo Fisher Scientific; 31985070). For
452 eVLPs prepared for protein or RNA quantification, or those that were injected into mice,
453 the filtered supernatant was concentrated 1500-fold by ultracentrifugation using a cushion
454 of 20% (w/v) sucrose in PBS. Ultracentrifugation was performed at 26,500 rpm (86,242
455 g) for 2 h (4ºC) using an SW32 Ti rotor in an Optima XE Ultracentrifuge (Beckman Coulter).
456 Following ultracentrifugation, eVLP pellets were resuspended in cold PBS pH 7.4 (Gibco;
457 10010023) and centrifuged at 1,000 g for 5 min to remove debris. eVLPs were frozen at
458 a rate of -1ºC/min and stored at -80ºC. eVLPs were thawed on ice immediately prior to
459 use.
460
461 **eVLP transduction and genomic DNA isolation**
462 Cells were transduced with eVLPs as described previously[8,22] with a few modifications.
463 Cells were plated for transduction in 96-well plates at a density of 16,000 cells per well.

After 20–24 h, eVLPs were added directly to the culture media in each well. In general, eVLPs were serially diluted by 2-fold to generate dose titration curves, and a constant volume of 5 µL of eVLP-containing solution was added to each well. 48–72 h post-transduction, cellular genomic DNA was isolated. Media was aspirated from each well, and 60 µL of lysis buffer (10 mM Tris-HCl pH 8.0, 0.05% SDS, 25 µg mL^{-1} Proteinase K (Thermo Fisher Scientific; EO0492)) was added to each well. Lysis was achieved by incubation at 37 ºC for 1–1.5 h followed by heat inactivation at 80ºC for 30 min.

High-throughput sequencing of genomic DNA

Genomic DNA was isolated as described above. Following genomic DNA isolation, 1 µL of the isolated DNA (1–10 ng) was used as input for the first of two PCR reactions. Genomic loci were amplified in PCR1 using Phusion U polymerase (Thermo Fisher Scientific; F562L). PCR1 primers are listed in Supplementary Table 2 under the HTS_forward and HTS_reverse columns. PCR1 was performed as follows: 95 ºC for 3 min; 30 cycles of 95 ºC for 15 s, 61 ºC for 20 s, and 72 ºC for 30s; 72ºC for 1 min. PCR1 products were confirmed on a 1% agarose gel. 1 µL of PCR1 was used as an input for PCR2 to install Illumina barcodes. PCR2 was conducted for nine cycles of amplification using Phusion HotStart II polymerase (Thermo Fisher Scientific; F537L). Following PCR2, samples were pooled and gel purified in a 1% agarose gel using a QIAquick Gel Extraction Kit (Qiagen; 28704). Library concentration was quantified using the Qubit High-Sensitivity Assay Kit (Thermo Fisher Scientific; Q33230). Samples were sequenced on an Illumina MiSeq instrument (paired-end read, read 1: 200–280 cycles, read 2: 0 cycles) using an Illumina MiSeq 300 v2 Kit (Illumina).

High-throughput sequencing data analysis for base editing experiments

Sequencing reads were demultiplexed using the MiSeq Reporter software (v2.6) (Illumina) and were analyzed using CRISPResso2 (ref. [41]) (v2.3.2) as previously described[8]. Batch analysis mode (one batch for each unique amplicon and sgRNA combination analyzed) was used in all cases. Reads were filtered by minimum average quality score (Q > 30) prior to analysis. The following quantification window parameters were used: -w 20 -wc -10. Base editing efficiencies are reported as the percentage of sequencing reads containing a given base conversion at a specific position. Prism 10 (GraphPad) was used to generate dot plots and bar plots.

Lentiviral vector production

Lentiviral vectors were constructed via Golden Gate cloning into the LentiCRISPRv2-Opti backbone, a gift from the Whitehead Institute Functional Genomics Platform (Addgene #163126). Plasmids were propagated in NEB® Stable (New England Biolabs; C3040H) chemically competent *E. coli*. Prior to lentiviral vector production, HEK293T/17 cells were maintained in antibiotic-free DMEM supplemented with 10% fetal bovine serum (v/v). On day 1, 5×10^6 cells were plated in 10 mL of media in T-75 flasks. The following day, cells were transfected with 6 µg of VSV-G envelope plasmid, 9 µg of psPAX2 (plasmid encoding viral packaging proteins) and 9 µg of transfer vector plasmid diluted in 1,500 µL Opti-MEM with 70 µL of FuGENE HD transfection reagent (Promega; E2312). Two days after transfection, media was centrifuged at 500 *g* for 5 min to remove cell debris followed by filtration using a 0.45-µm PVDF vacuum filter (Millipore; SE1M003M00). The filtered

510 supernatant was concentrated using PEG-it Virus Precipitation Solution (System
511 Biosciences; LV825A-1) according to the manufacturer's protocols and resuspended in
512 Opti-MEM serum-free media (Gibco; 31985070).
513
514 **sgRNA library propagation**
515 For the genome-wide knockout screen, a previously described human genome-wide
516 sgRNA library containing 98,077 unique sgRNAs targeting 19,707 genes across the
517 human genome[24] was obtained as a gift from the Whitehead Institute Functional
518 Genomics Platform. sgRNA sequences are listed in Supplementary Table 3. Vectors
519 contained pU6-sgRNA expression cassettes along with pEFS-Cas9-P2A-PuroR
520 (LentiCRISPRv2-Opti backbone, Addgene #163126). The plasmid library was
521 propagated as follows. First, electrocompetent cells were generated from NEB® Stable
522 (New England Biolabs; C3040H) chemically competent *E. coli* by growing single colonies
523 to mid-log phase in LB media containing 10 µg/mL tetracycline and 50 µg/mL
524 streptomycin, collecting cells by centrifugation at 5,000 g for 1 min at 4 ºC, washing with
525 cold 10% (v/v) glycerol, and repeating for a total of four washes. Freshly prepared
526 electrocompetent cells were transferred to a chilled 0.1 cm electroporation cuvette (Bio-
527 Rad; 1652089) and mixed with the purified, assembled library plasmids. Cells were
528 electroporated using a time-constant protocol with t = 5 ms at 1.5 kV. Electroporated cells
529 were recovered at 37 ºC for 25 min with shaking. Recovered cells were plated onto 500
530 cm^2 plates containing LB media + 1.5% agar supplemented with 100 µg/mL carbenicillin
531 and incubated for 16 h at 37 ºC. After overnight incubation, colonies were scraped into
532 LB media and cells were collected by centrifugation. Plasmids were purified using a
533 Plasmid Plus Maxi Kit (Qiagen; 12963) according to the manufacturer's protocols. sgRNA
534 representation in the propagated plasmid library was confirmed via targeted amplicon
535 sequencing.
536
537 **Genome-wide knockout screen for cargo-loaded eVLP production**
538 Lentiviral libraries were produced as described above and were concentrated ~66-fold by
539 PEG precipitation. Gesicle cells were seeded at a density of 1.5×10^7 cells per T-175 and
540 immediately transduced with 105 µL of concentrated lentivirus. A total of 2.4×10^8 Gesicle
541 cells were seeded for transduction. 24 h after transduction, cells were trypsinized and
542 reseeded at half the original density in media supplemented with 2 µg/mL puromycin.
543 Puromycin selection was continued for 7 days, during which time cell viability was
544 monitored and cells were expanded upon reaching confluency. The initial multiplicity of
545 infection (MOI) was inferred by counting surviving cells and assuming a doubling time of
546 24 h. Using this method, the MOI was calculated to be 0.28, corresponding to
547 approximately 660x coverage of the sgRNA library. A minimum of 1×10^8 cells were carried
548 forward each time the cells were passaged to retain overall coverage.
549 After cells were robustly surviving puromycin selection (~1 week), cells were
550 seeded for eVLP production in T-75 flasks at a density of 5×10^6 cells/flask. At this time,
551 1×10^8 cells were collected by centrifugation, and the cell pellet was frozen at -80ºC and
552 reserved for RNA extraction (see below). 24 h after seeding, cells were transfected using
553 the jetPRIME transfection reagent (Polyplus; 114-75) according to the manufacturer's
554 protocols. A mixture of pUC19 (4,400 ng), VSV-G (400 ng), MMLV gag-pro-pol (3,375 ng),
555 and MMLVgag–ABE8e (1,125) plasmids were co-transfected per T-75 flask. 42 h post

556 transfection, eVLPs were harvested and filtered as described above. The filtered
557 supernatant was concentrated by sucrose-cushion ultracentrifugation as described above.
558 Following ultracentrifugation, eVLP pellets were resuspended in cold PBS pH 7.4 (Gibco;
559 10010023). Purified eVLPs were treated with DNase (Qiagen; 79254) followed by RNA
560 extraction using the QIAmp Viral RNA Mini Kit (Qiagen; 52904) according to the
561 manufacturer's protocols. RNA was extracted from the producer-cell pellet using QIAzol
562 Lysis Reagent (Qiagen; 79306) according to the manufacturer's protocols. This entire
563 process of seeding single-knockout Gesicle cells followed by eVLP production and RNA
564 extractions was performed twice on different days for two screen replicates.
565 Following RNA extraction, both producer-cell and eVLP RNA were reverse
566 transcribed using the Maxima Reverse Transcriptase (Thermo Fisher Scientific; EP0742)
567 according to the manufacturer's protocols. Primers and other oligonucleotides used for
568 target-primed sgRNA reverse transcription are listed in Supplementary Table 1. The RT
569 primer was added at a final concentration of 1 μM in the RT reaction. Following incubation
570 at 50ºC for 20 min, the template-switching oligo (TSO) was spiked in to the reaction at a
571 final concentration of 1 μM. The reaction was incubated for a further 20 min at 50ºC, and
572 heat inactivated at 85ºC for 5 min. For producer-cell RNA only, the RT products were
573 further processed by hydrolyzing the RNA in 0.2 M NaOH (final concentration) and
574 heating at 90ºC for 10 min, cleaning up with the MinElute Reaction Cleanup Kit (Qiagen;
575 28104) according to the manufacturer's protocols, and left size selection using SPRIselect
576 (Beckman Coulter; B23317) at a 1.5x bead ratio to remove smaller products and residual
577 primers. Producer-cell cDNAs were subsequently amplified for sequencing with the KAPA
578 HiFi HotStart ReadyMix (Roche Diagnostics; 09420398001) using 2.5 μL of cDNA input
579 per 25 μL reaction and the following conditions: 95 ºC for 3 min; 20 cycles of 98 ºC for 20
580 s, 61 ºC for 20 s, and 72 ºC for 30s; 72ºC for 2 min. eVLP cDNAs were amplified for
581 sequencing with the KAPA HiFi HotStart ReadyMix using 2.5 μL of cDNA input per 25 μL
582 reaction and the following conditions: 95 ºC for 3 min; 14 cycles of 98 ºC for 20 s, 61 ºC
583 for 20 s, and 72 ºC for 30s; 72ºC for 2 min. Illumina barcodes were installed using KAPA
584 HiFi HotStart ReadyMix using 2 μL of PCR1 input per 25 μL reaction and the following
585 conditions: 95 ºC for 3 min; 9 cycles of 98 ºC for 20 s, 61 ºC for 20 s, and 72 ºC for 30s;
586 72ºC for 2 min. Following PCR2, samples were gel purified in a 1% agarose gel using a
587 QIAquick Gel Extraction Kit (Qiagen; 28704). Library concentration was quantified using
588 the Qubit High-Sensitivity Assay Kit (Thermo Fisher Scientific; Q33230). Samples were
589 sequenced on an Illumina NextSeq instrument (paired-end read, read 1: 76 cycles, read
590 2: 0 cycles) using an Illumina NextSeq 75-cycle High-Output v2.5 Kit (Illumina).
591
592 **Genome-wide knockout screen analysis**
593 Code used for processing sequencing reads from the genome-wide knockout screen is
594 provided in Supplementary Note 1. Briefly, sequencing reads were demultiplexed using
595 bcl2fastq (v2.20.0.422). Reads were trimmed using seqkit[42] (v2.6.1) to restrict analysis to
596 the UMI and sgRNA protospacer sequences only. Then, reads were UMI-deduplicated
597 using AmpUMI[43] and trimmed with seqkit to remove the UMI and restrict subsequent
598 analysis to the sgRNA protospacer sequences only. Processed reads were aligned to a
599 reference fasta file containing all sgRNA sequences using bowtie[44] (v1.3.1), and sgRNA
600 counts were generated from alignments as previously described[24]. Raw sgRNA counts
601 are provided in Supplementary Table 4. MAGeCK[45] (v0.5.9.5) was used to quantify gene-

602 level phenotypes from the sgRNA counts. Producer-cell samples were treated as "control"
603 samples and eVLP samples were treated as "treatment" samples for the purpose of
604 MAGeCK analysis. Median-normalized sgRNA read counts and fold changes are
605 provided in Supplementary Table 5, and gene-level phenotypes are provided in
606 Supplementary Table 6. For genes with a positive median $\log_2$ fold change, the positive
607 MAGeCK RRA score, p-value, and FDR were used, and for genes with a negative median
608 $\log_2$ fold change, the negative MAGeCK RRA score, p-value, and FDR were used. Prism
609 10 (GraphPad) was used to generate dot plots.
610
611 **Generation of knockout cell lines**
612 To generate knockout cell lines via Cas9/sgRNA lentiviral transduction, lentiviral vectors
613 were cloned and produced as described above. Cells were seeded in T-75 flasks at a
614 density of 5×10^6 cells/flask and immediately transduced with 50 µL of concentrated
615 lentivirus. 24 h after transduction, cells were trypsinized and reseeded in media
616 supplemented with 2 µg/mL puromycin. Puromycin selection was continued, during which
617 time cell viability was monitored and cells were expanded upon reaching confluency. After
618 cells were robustly surviving puromycin selection (~1 week), cells were harvested and
619 genotyped via targeted-amplicon high-throughput sequencing as described above to
620 confirm gene knockout. Cell lines were regularly genotyped over time to confirm
621 continued gene knockout.
622 To generate knockout cell lines via Cas9-eVLP transduction, v4 Cas9-eVLPs were
623 produced as described above. Cells were seeded in 96-well plates at a density of 16,000
624 cells per well. 24 h after seeding, cells were transduced with 5 µL of purified Cas9-eVLPs
625 per well. 72 h after eVLP transduction, cells were harvested and genotyped via targeted-
626 amplicon high-throughput sequencing as described above to confirm gene knockout.
627 Cells were expanded and regularly genotyped over time to confirm continued gene
628 knockout.
629
630 **eVLP-packaged sgRNA extraction and RT-qPCR**
631 eVLPs for RNA extraction were purified via sucrose-cushion ultracentrifugation as
632 described above. Purified eVLPs were treated with DNase (Qiagen; 79254) followed by
633 RNA extraction using the QIAmp Viral RNA Mini Kit (Qiagen; 52904) according to the
634 manufacturer's protocols. Extracted RNA was reverse transcribed using SuperScript™ III
635 First-Strand Synthesis SuperMix (Thermo Fisher Scientific; 18080400) and an sgRNA-
636 specific DNA primer (see Supplementary Table 1) according to the manufacturer's
637 protocols. qPCR analysis of the resulting cDNA was performed using a QuantStudio™ 3
638 Real-Time PCR System (Thermo Fisher Scientific) with SYBR green dye (Lonza; 50512).
639 The relative eVLP-packaged sgRNA abundance was calculated as $\log_2$[fold change] (ΔC_t)
640 relative to control eVLPs (i.e. those produced from standard or *AAVS1*-knockout cells).
641
642 **Producer-cell RNA extraction and RT-qPCR**
643 Cellular RNA was extracted using the RNeasy Plus Mini Kit (Qiagen; 74136) according
644 to the manufacturer's protocols. Extracted RNA was reverse transcribed using
645 SuperScript™ III First-Strand Synthesis SuperMix (Thermo Fisher Scientific; 18080400)
646 using random hexamer primers according to the manufacturer's protocols. qPCR analysis
647 of the resulting cDNA was performed using a QuantStudio™ 3 Real-Time PCR System

(Thermo Fisher Scientific) with SYBR green dye (Lonza; 50512). The relative Cas9 mRNA abundance across different producer cells was calculated via the $\Delta\Delta C_t$ method using *ACTB* as the housekeeping gene. qPCR primers are listed in Supplementary Table 1.

Producer-cell protein extraction and Western blot analyses

For producer-cell protein extraction, 1×10^6 cells were collected by centrifugation at 500 g for 5 min. Cell pellets were washed once with 1 mL of cold PBS and lysed using RIPA buffer (Thermo Fisher Scientific; 89901) supplemented with cOmplete™ protease inhibitor cocktail (Roche Diagnostics; 11836153001) according to the manufacturer's protocols. Cells were lysed at 4ºC for 30 min with gentle agitation. The lysate was clarified by centrifugation at 10,000 g for 20 min at 4ºC, and the clarified supernatant was combined with 4x Laemmli Sample Buffer (Bio-Rad; 1610747) and heated at 95ºC for 10 min. Protein extracts were subsequently separated by electrophoresis at 150 V for 45 min on a NuPAGE 3–8% Tris-Acetate gel (Thermo Fisher Scientific; EA0378BOX) in 1x NuPAGE Tris-Acetate SDS running buffer (Thermo Fisher Scientific; LA0041). Transfer to a PVDF membrane was performed using an iBlot 2 Gel Transfer Device (Thermo Fisher Scientific) at 20 V for 7 min. The membrane was blocked for 1 h at room temperature with rocking in blocking buffer: 1% bovine serum albumin (BSA) and 0.1% Tween-20 in TBS (150 mM NaCl and 50 mM Tris-HCl). After blocking, the membrane was incubated overnight at 4ºC with rocking with mouse anti-Cas9 (Cell Signaling Technology; 14697, 1:1000 dilution) and rabbit anti-actin (Cell Signaling Technology; 4970, 1:1000 dilution). The membrane was washed three times with 1xTBST (150 mM NaCl, 0.5% Tween-20, and 50 mM Tris-HCl) for 10 min each time at room temperature, then incubated with goat anti-mouse secondary antibody (LI-COR IRDye 680RD; 926-68070, 1:10000 dilution in blocking buffer) and goat anti-rabbit secondary antibody (LI-COR IRDye 800CW; 926-32211, 1:10000 dilution in blocking buffer) for 1 h at room temperature with rocking. The membrane was washed as before and imaged using an Odyssey Imaging System (LI-COR). Protein abundances were quantified by densitometry using ImageJ (v2.14.0). Cas9 abundances were normalized to the actin abundance within each sample, and comparisons across samples were performed using these actin-normalized values.

For protein extraction from cells transfected with eVLP production plasmids, cells were first seeded for eVLP production in T-75 flasks as described above. 24 h after seeding, cells were transfected with all eVLP production plasmids except the VSV-G plasmid. 48 h after transfection, cells were trypsinized and collected by centrifugation, and were then processed as described above.

eVLP protein content quantification

eVLP protein content quantification was performed as described previously[8]. Briefly, ultracentrifuge-purified eVLPs were lysed in dye-free Laemmli sample buffer (50 mM Tris-HCl pH 7.0, 2% sodium dodecyl sulfate (SDS), 10% (v/v) glycerol, 2 mM dithiothreitol (DTT)) by heating at 95ºC for 15 min. The concentration of ABE protein in purified eVLPs was quantified using the FastScan™ Cas9 (*S. pyogenes*) ELISA kit (Cell Signaling Technology; 29666C) according to the manufacturer's protocols. Recombinant Cas9 (*S. pyogenes*) nuclease protein (New England Biolabs; M0386) was used to generate the standard curve for quantification. The concentration of MLV p30 protein in purified eVLPs

694 was quantified using the MuLV Core Antigen ELISA kit (Cell Biolabs; VPK-156) according
695 to the manufacturer's protocols. The number of ABE protein molecules per eVLP was
696 calculated by determining the ratio of Cas9 molecules to p30 molecules and assuming a
697 copy number of 1800 molecules of p30 per eVLP as previously described[8].
698
699 **Animal experiments**
700 All mouse experiments were compliant with relevant ethical regulations and were
701 approved by the MIT Committee on Animal Care (D16-00078; 2402000629). Wild-type 8-
702 week-old adult male C57BL/6J mice (000664) were purchased from the Jackson
703 Laboratory. All mice were housed in a room maintained on a 12 h light and dark cycle
704 with *ad libitum* access to standard rodent diet and water. Animals were randomly
705 assigned to various experimental groups.
706 Retro-orbital injections were performed as described previously[8] with a few
707 modifications. eVLPs for retro-orbital injections were purified via sucrose-cushion
708 ultracentrifugation as described above. Immediately prior to injection, eVLPs were
709 partially clarified by centrifugation at 1000 g for 5 min to remove debris. The eVLP-
710 containing supernatant was diluted with 0.9% NaCl (Hospira; 00409-4888-10), and a total
711 of 100 μL solution (containing 15 μL of 1500-fold concentrated purified eVLPs,
712 approximately 3×10^{11} eVLPs) was injected per mouse. Genomic DNA was purified from
713 bulk liver tissue using the Agencourt DNAdvance kit (Beckman Coulter; A48705)
714 according to the manufacturer's protocols. Purified genomic DNA was amplified for high-
715 throughput sequencing as described above, with 25 cycles of amplification during PCR1.
716
717 **ENVLPE$^+$ production**
718 ENVLPE$^+$ particles[10] were produced analogously to eVLPs. Producer cells were seeded
719 in T-75 flasks at a density of 5×10^6 cells per flask. After 20–24 h, cells were transfected
720 using the jetPRIME transfection reagent (Polyplus; 114-75) according to the
721 manufacturer's protocols. A mixture of plasmids expressing VSV-G (1550 ng), psPAX2-
722 D64V (1,149 ng; Addgene #63586, a gift from David Rawlings & Andrew Scharenberg),
723 pCMV_ENVLPE+ (665 ng; Addgene #232427, a gift from Gil Westmeyer),
724 pCMV_ABE8e_superNLS (1,023 ng; Addgene #232429, a gift from Gil Westmeyer), and
725 a *BCL11A*-targeting PP7-containing sgRNA (4,913 ng; cloned from Addgene #232432, a
726 gift from Gil Westmeyer) were co-transfected per T-75 flask. 40–48 h post-transfection,
727 producer cell supernatant was harvested and centrifuged for 5 min at 500 g to remove
728 cell debris. The clarified ENVLPE$^+$-containing supernatant was filtered through a 0.45-μm
729 PVDF filter (Millipore; SE1M003M00). The filtered supernatant was concentrated 100-fold
730 using PEG-it Virus Precipitation Solution (System Biosciences; LV825A-1) according to
731 the manufacturer's protocols and resuspended in Opti-MEM serum-free media (Thermo
732 Fisher Scientific; 31985070).
733
734 **Statistical analysis**
735 Data are presented as mean and standard deviation (s.d.). No statistical methods were
736 used to predetermine sample size. Statistical analysis was performed using GraphPad
737 Prism software. Sample sizes are described in the figure legends.
738
739 **Data availability**

The high-throughput sequencing data generated during this study is being deposited at the NCBI Sequence Read Archive database under PRJNA1288558. Raw data from the genome-wide knockout screen is provided in Supplementary Tables 3–6. Key plasmids from this work will be deposited to Addgene for distribution. Other plasmids and cell lines are available from the corresponding author on request.

Code availability

The code used for analyzing base editing efficiencies are available at https://github.com/pinellolab/CRISPResso2. The code used for analyzing CRISPR screen results are available in Supplementary Note 1 and at https://sourceforge.net/p/mageck/wiki/Home/.

Acknowledgements

This work was supported by the Whitehead Institute and Whitehead Fellows Program (A.R.); NIH Director's Early Independence Award DP5OD037342 (A.R.); Merkin Institute for Transformative Technologies in Healthcare (A.R.); McGuire Family Foundation (A.R.); and the James M. and Cathleen D. Stone Foundation (A.R.). H.J. acknowledges support from the National Research Foundation of Korea. A.S. was supported by the Whitehead Scholars Program at Williams College. We thank H. Keys and the Functional Genomics Platform at Whitehead Institute for providing the genome-wide sgRNA library used in our study; A. Nelson, D. Liu, and the Whitehead Genome Technology Core for access to Illumina sequencing instrumentation; and the Jain, Reddien, Weissman, and Young Labs for generous access to equipment.

Author contributions

A.R. conceived the project. D.L., H.J., A.G., A.S., and A.R. designed the research, performed experiments, and analyzed data. H.J. performed mouse experiments. A.R. wrote the manuscript, and all authors edited the manuscript.

Competing interests

The authors declare competing financial interests: D.L. and A.R. have filed a patent application on this work through the Whitehead Institute. The remaining authors declare no competing interests.

References

1. Raguram, A., Banskota, S. & Liu, D.R. Therapeutic in vivo delivery of gene editing agents. *Cell* **185**, 2806-2827 (2022).
2. van Haasteren, J., Li, J., Scheideler, O.J., Murthy, N. & Schaffer, D.V. The delivery challenge: fulfilling the promise of therapeutic genome editing. *Nat Biotechnol* **38**, 845-855 (2020).
3. Wang, D., Zhang, F. & Gao, G. CRISPR-Based Therapeutic Genome Editing: Strategies and In Vivo Delivery by AAV Vectors. *Cell* **181**, 136-150 (2020).
4. Wei, T. et al. Delivery of Tissue-Targeted Scalpels: Opportunities and Challenges for In Vivo CRISPR/Cas-Based Genome Editing. *ACS Nano* **14**, 9243-9262 (2020).
5. Wang, J.Y. & Doudna, J.A. CRISPR technology: A decade of genome editing is only the beginning. *Science* **379**, eadd8643 (2023).
6. Tsuchida, C.A., Wasko, K.M., Hamilton, J.R. & Doudna, J.A. Targeted nonviral delivery of genome editors in vivo. *Proc Natl Acad Sci U S A* **121**, e2307796121 (2024).
7. An, M. et al. Engineered virus-like particles for transient delivery of prime editor ribonucleoprotein complexes in vivo. *Nat Biotechnol* **42**, 1526-1537 (2024).
8. Banskota, S. et al. Engineered virus-like particles for efficient in vivo delivery of therapeutic proteins. *Cell* **185**, 250-265 e216 (2022).
9. Choi, J.G. et al. Lentivirus pre-packed with Cas9 protein for safer gene editing. *Gene Ther* **23**, 627-633 (2016).
10. Geilenkeuser, J. et al. Engineered nucleocytosolic vehicles for loading of programmable editors. *Cell* **188**, 2637-2655 e2631 (2025).
11. Haldrup, J. et al. Engineered lentivirus-derived nanoparticles (LVNPs) for delivery of CRISPR/Cas ribonucleoprotein complexes supporting base editing, prime editing and in vivo gene modification. *Nucleic Acids Res* **51**, 10059-10074 (2023).
12. Halegua, T. et al. Delivery of Prime editing in human stem cells using pseudoviral NanoScribes particles. *Nat Commun* **16**, 397 (2025).
13. Hamilton, J.R. et al. In vivo human T cell engineering with enveloped delivery vehicles. *Nat Biotechnol* **42**, 1684-1692 (2024).
14. Hamilton, J.R. et al. Targeted delivery of CRISPR-Cas9 and transgenes enables complex immune cell engineering. *Cell Rep* **35**, 109207 (2021).
15. Indikova, I. & Indik, S. Highly efficient 'hit-and-run' genome editing with unconcentrated lentivectors carrying Vpr.Prot.Cas9 protein produced from RRE-containing transcripts. *Nucleic Acids Res* **48**, 8178-8187 (2020).
16. Ling, S. et al. Customizable virus-like particles deliver CRISPR-Cas9 ribonucleoprotein for effective ocular neovascular and Huntington's disease gene therapy. *Nat Nanotechnol* **20**, 543-553 (2025).

812 17. Lu, Z. et al. Lentiviral Capsid-Mediated Streptococcus pyogenes Cas9
813 Ribonucleoprotein Delivery for Efficient and Safe Multiplex Genome Editing.
814 *CRISPR J* **4**, 914-928 (2021).

815 18. Lyu, P., Javidi-Parsijani, P., Atala, A. & Lu, B. Delivering Cas9/sgRNA
816 ribonucleoprotein (RNP) by lentiviral capsid-based bionanoparticles for efficient 'hit-
817 and-run' genome editing. *Nucleic Acids Res* **47**, e99 (2019).

818 19. Lyu, P. et al. Adenine Base Editor Ribonucleoproteins Delivered by Lentivirus-Like
819 Particles Show High On-Target Base Editing and Undetectable RNA Off-Target
820 Activities. *CRISPR J* **4**, 69-81 (2021).

821 20. Lyu, P., Wang, L. & Lu, B. Virus-Like Particle Mediated CRISPR/Cas9 Delivery for
822 Efficient and Safe Genome Editing. *Life (Basel)* **10** (2020).

823 21. Mangeot, P.E. et al. Genome editing in primary cells and in vivo using viral-derived
824 Nanoblades loaded with Cas9-sgRNA ribonucleoproteins. *Nat Commun* **10**, 45
825 (2019).

826 22. Raguram, A., An, M., Chen, P.Z. & Liu, D.R. Directed evolution of engineered virus-
827 like particles with improved production and transduction efficiencies. *Nat Biotechnol*
828 (2024).

829 23. Xu, D. et al. Programmable epigenome editing by transient delivery of CRISPR
830 epigenome editor ribonucleoproteins. *Nat Commun* **16**, 7948 (2025).

831 24. Lam, B. et al. Multi-species genome-wide CRISPR screens identify conserved
832 suppressors of cold-induced cell death. *bioRxiv* (2024).

833 25. Replogle, J.M. et al. Combinatorial single-cell CRISPR screens by direct guide RNA
834 capture and targeted sequencing. *Nat Biotechnol* **38**, 954-961 (2020).

835 26. Seczynska, M., Bloor, S., Cuesta, S.M. & Lehner, P.J. Genome surveillance by
836 HUSH-mediated silencing of intronless mobile elements. *Nature* **601**, 440-445
837 (2022).

838 27. Seczynska, M. & Lehner, P.J. The sound of silence: mechanisms and implications
839 of HUSH complex function. *Trends Genet* **39**, 251-267 (2023).

840 28. DeKelver, R.C. et al. Functional genomics, proteomics, and regulatory DNA
841 analysis in isogenic settings using zinc finger nuclease-driven transgenesis into a
842 safe harbor locus in the human genome. *Genome Res* **20**, 1133-1142 (2010).

843 29. Liao, J. et al. Therapeutic adenine base editing of human hematopoietic stem cells.
844 *Nat Commun* **14**, 207 (2023).

845 30. Johnson, S.S., Zhang, C., Fromm, J., Willis, I.M. & Johnson, D.L. Mammalian Maf1
846 is a negative regulator of transcription by all three nuclear RNA polymerases. *Mol*
847 *Cell* **26**, 367-379 (2007).

848 31. Vannini, A. et al. Molecular basis of RNA polymerase III transcription repression by
849 Maf1. *Cell* **143**, 59-70 (2010).

850 32. Vorlander, M.K. et al. Structural basis for RNA polymerase III transcription
851 repression by Maf1. *Nat Struct Mol Biol* **27**, 229-232 (2020).

852 33. Musunuru, K. et al. In vivo CRISPR base editing of PCSK9 durably lowers
853 cholesterol in primates. *Nature* **593**, 429-434 (2021).

854 34. Richter, M.F. et al. Phage-assisted evolution of an adenine base editor with
855 improved Cas domain compatibility and activity. *Nat Biotechnol* **38**, 883-891 (2020).

856 35. Neugebauer, M.E. et al. Evolution of an adenine base editor into a small, efficient
857 cytosine base editor with low off-target activity. *Nat Biotechnol* **41**, 673-685 (2023).

858 36. Levy, J.M. et al. Cytosine and adenine base editing of the brain, liver, retina, heart
859 and skeletal muscle of mice via adeno-associated viruses. *Nat Biomed Eng* **4**, 97-
860 110 (2020).

861 37. Montagna, C. et al. VSV-G-Enveloped Vesicles for Traceless Delivery of CRISPR-
862 Cas9. *Mol Ther Nucleic Acids* **12**, 453-462 (2018).

863 38. Kunitake, K. et al. Barcoding of small extracellular vesicles with CRISPR-gRNA
864 enables comprehensive, subpopulation-specific analysis of their biogenesis and
865 release regulators. *Nat Commun* **15**, 9777 (2024).

866 39. Lu, A. et al. Genome-wide interrogation of extracellular vesicle biology using
867 barcoded miRNAs. *Elife* **7** (2018).

868 40. Strebinger, D. et al. Cell type-specific delivery by modular envelope design. *Nat*
869 *Commun* **14**, 5141 (2023).

870 41. Clement, K. et al. CRISPResso2 provides accurate and rapid genome editing
871 sequence analysis. *Nat Biotechnol* **37**, 224-226 (2019).

872 42. Shen, W., Le, S., Li, Y. & Hu, F. SeqKit: A Cross-Platform and Ultrafast Toolkit for
873 FASTA/Q File Manipulation. *PLoS One* **11**, e0163962 (2016).

874 43. Clement, K., Farouni, R., Bauer, D.E. & Pinello, L. AmpUMI: design and analysis of
875 unique molecular identifiers for deep amplicon sequencing. *Bioinformatics* **34**, i202-
876 i210 (2018).

877 44. Langmead, B., Trapnell, C., Pop, M. & Salzberg, S.L. Ultrafast and memory-efficient
878 alignment of short DNA sequences to the human genome. *Genome Biol* **10**, R25
879 (2009).

880 45. Li, W. et al. MAGeCK enables robust identification of essential genes from genome-
881 scale CRISPR/Cas9 knockout screens. *Genome Biol* **15**, 554 (2014).

882